Aerodynamic Investigation of Novel Toroidal Joined Blade Tips Propeller

Kangni Combey[1], Hajar Chouiyakh[1], Khaoula Qaissi[1], Mustapha Faqir[1]and Omer A. Elsayed[1,2]

[1]School of Aerospace and Automotive Engineering, College of Engineering and Architecture, LERMA Lab, International University of Rabat, Morocco
[2]*omer.almatbagi@uir.ac.ma*

Abstract

This article investigates the aerodynamic performance of a novel propeller design named the Toroidal Joined Blade Tips (T-JBT) propeller. The T-JBT propeller blade comprises two conventional blades interconnected at their tips on the midplane to form a continuous looped blade structure. Inspired by the concept of a ring-wing aircraft, the goal of this design is to reduce propeller noise by eliminating tip vortices while maintaining aerodynamic performance. Numerical simulations were conducted to compare the aerodynamic performance of the T-JBT propeller with that of a conventional propeller. The results showed that under the considered operating conditions, the T-JBT propeller generates higher thrust and torque. The absence of tip vortices in the T-JBT enabled improved thrust through reduced losses. However, the flow visualizations revealed a complex flow structure, with a higher acceleration of the flow behind the toroidal propeller compared to the conventional propeller and high-speed flow at the region between the low-pressure side of the forward blade and the high-pressure side of the rearward blade. For the considered operating condition, the flow mainly remains attached due to the generated turbulent layer. This initial T-JBT design shows promise for improving aerodynamic performance.

Keywords: Propeller design, Toroidal propeller, Joined blade tips, Urban air mobility, eVTOL aircraft.

1 Introduction

Scientific and technological evolution has led to a surge in energy requirements, urbanization, and a growing number of vehicles on the roads. The high number of vehicles on the roads has resulted in several issues, including traffic congestion. This congestion causes longer and delayed travel times, higher carbon emissions, and exacerbates climate problems. To tackle both energy scarcity and mitigate climate change impacts, it is feasible to envision a future of transportation that embraces green technologies, specifically electric alternative to fossil fuels. Public transportation systems like buses and high-speed trains can help alleviate these issues by adopting enhanced electrical technology and with appropriate transit infrastructure. However, in densely populated cities with limited space for new infrastructure development, relying solely on green terrestrial public transport may not offer a comprehensive solution. Consequently, the concept of Urban Air Mobility (UAM) has emerged, wherein intercity and intracity transportation will be facilitated by Electric Vertical Take-Off and Landing (eVTOL) aircraft [1, 2]. eVTOL has emerged as potential solution to address the increasing demand for UAM. These innovative aircraft are being designed to operate a large range of missions, including upon request taxi services [3], air ambulances, emergency supply delivery, organ transport [4], and scheduled airline excursions. They offer more flexible trajectories than cars and trains [5], and they only require start and end points infrastructures, called vertiports.

Positioned between helicopters and drones in terms of technology, these eVTOLs aircraft necessitate special considerations in the design process, primarily due to the potential noise they may generate. Propellers play a crucial role in UAM, with special attention to the tip vortex effect, as it significantly influences induced drag [6] and noise levels. Optimizing propellers for specific applications is essential, and there exist numerous methods to

achieve this. One avenue for optimizing propellers is through shape optimization [7, 8] and employing Distributive Electric Propulsion (DEP) system [9, 10]. Incorporating multirotor with smaller diameters is a deliberate choice to mitigate the noise produced by the rotating blades. While these smaller diameters can generate total thrust equivalent to that of a larger rotor, the overall noise is significantly reduced. The adoption of smaller rotors not only decreases noise but also enhances the overall stability of the aircraft [11]. This is achieved through redundancy between the rotors and independent control of each motor, offering precise control over position and orientation of the vehicle [12]. Additionally, smaller rotors contribute to increased safety in urban environments, as they are less likely to cause damage in the event of contact with infrastructure or people. Moreover, the use of smaller rotors requires less power to lift the aircraft, making them well-suited for eVTOL applications.

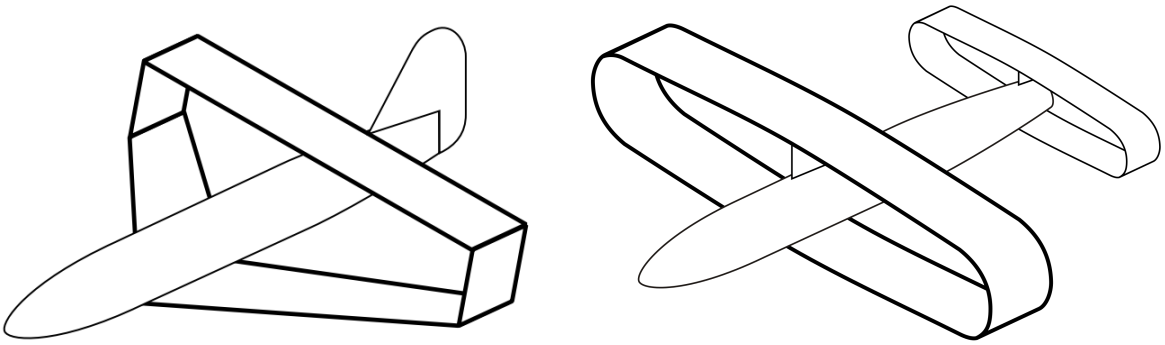

(a) Box Wing [13] (b) Ring Wing [13]

Figure 1: Conceptual Design of a) Box Wing and b) Ring Wing

Numerous aerospace startups and companies worldwide are actively contributing to transform the idea of UAM from fiction into reality. In this ambitious pursuit, a diverse array of approaches is being explored. Some entities opt for conventional propeller blades on multirotor eVTOL aircraft, while others focus on unconventional propeller designs. The latter aims to reduce propeller noise while maintaining or improving overall aerial vehicle performance. One remarkable concept is the "Joined Blades" design, drawing inspiration from early 1900s joined wing (also called closed wing) aircraft concept. An example is the Blériot III (1906) [14], featuring a ring-wing configuration. Despite not achieving flight, it serves as a historical inspiration for investigations and understanding of the physics of the flow around such wing configurations.

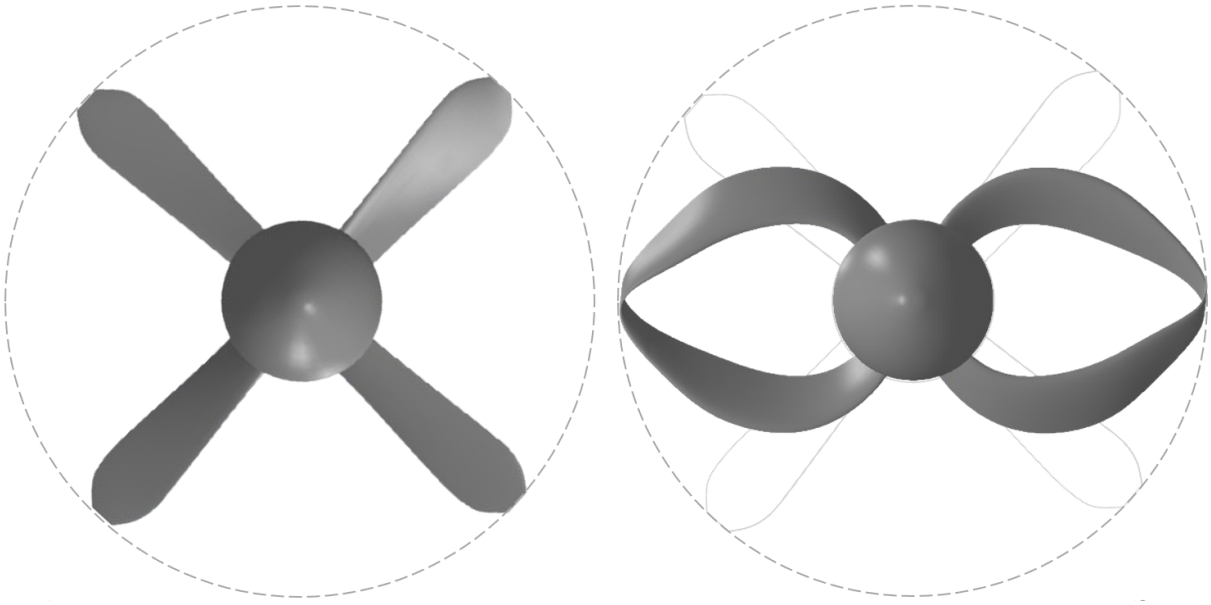

(a) Conventional F29 Propeller (b) T-JBT Propeller

Figure 2: Comparison between a) Conventional F29 Propeller b) T-JBT Propeller

One of the key aspects that researchers have investigated in the realm of joined blades propellers is the influence of looped blades on the acoustics signal. Jianwei Sun et al. [15] have demonstrated that the loop-type propeller shows a comparatively higher aeroacoustics performance compare to conventional DJI Phantom III propeller and presents notable characteristics in the tonal noise components for harmonics suppression. Joining the blades, was demonstrated that it has the potential to suppress the tip vortex [16, 15]. Joined blade propeller named "Toroidal propeller" was proposed by researchers from MIT Lincoln Laboratory [17]. In this design, two blades are interconnected in a loop-like structure. According to the authors, this concept is anticipated to significantly decrease noise levels when compared to traditional propellers. This novel approach represents a significant stride in the ongoing quest to advance eVTOL technology and ultimately facilitate the practical implementation of UAM solutions in densely populated urban environments.

This concept draws inspiration from the idea of box and ring wing aircraft, where the two wings of the aircraft are connected to form a loop, so there is no wingtips, as shown in Fig. 1. The "looped-wing" concept, is extended to rotating wings (see Fig. 2). This research delves into design and aerodynamics analysis of novel propeller, particularly the Joined Blades concept named Toroidal Joined Blade Tips (T-JBT) propeller, in the context of advancing UAM technologies. The T-JBT propeller comprises two conventional blades that are interconnected at their tips, creating a looped blade structure.

2 T-JBT Propeller Design

The design goal of the T-JBT propeller is to have a propeller that will be able to achieve excellent noise reduction while keeping good aerodynamic performance, particularly for eVTOL applications. The design must satisfy structural requirements as well as manufacturing constraints. Although detailed structural analyses are not carried out in this study, the loop-type blade is expected to offer higher structural rigidity.

The T-JBT is expected to operate from low speed (takeoff) to climb and cruise. In this design, the propeller is considered fixed-pitch for the initial analysis, however pitch control can be achieved by connecting the two blade roots to a common base, which can rotate to ensure proper alignment with the flow. The absence of a tip in the joined blades propeller, eliminates tip vortex-related consequences, including noise, as demonstrated by MIT researchers [17]. Hence, this study aims to conduct an aerodynamic investigation of the self-designed looped blade propeller named T-JBT propeller.

3 Propeller Performance Parameters

The propeller performance can be specified in terms of non dimensional quantities such as, advance ration J, thrust coefficient C_T, torque coefficient C_Q, power coefficient C_P and propeller efficiency η_p, as defined in the Equations 1 to 4. The Activity Factor (AF) indicates how well a propeller can absorb power, and it depends on the ratio of blade area to the total area of the propeller disk. It quantifies how effectively the propeller blades use the available area of the propeller disc to absorb power [18]. For a single blade, AF_b can be found using the Equation 5. The (c/R_p) is function of the non-dimensional distance $x = r/R_p$, representing the radial position. To obtain the total activity factor of the propeller, simply multiply AF_b by the number of blades B.

$$J = \frac{V_\infty}{nD_p} \tag{1}$$

$$C_T = \frac{T}{\rho_\infty n^2 {D_p}^4} \tag{2}$$

$$C_Q = \frac{Q}{\rho_\infty n^2 {D_p}^5} \tag{3}$$

$$C_P = \frac{P}{\rho_\infty n^3 {D_p}^5} \tag{4}$$

$$AF_b = \frac{10^5}{32} \int_{R_h}^{R_{tip}} \left(\frac{c}{R_p}\right) x^3 \, dx \tag{5}$$

4 Geometry of the T-JBT Propeller

The novel T-JBT propeller, derives its name from the distinctive shape obtained by joining the tips of two conventional blades to create a looped blade in a toroidal form. The process involves connecting the tips of two adjacent blades of a conventional propeller (see Fig.2a) at their mid-plane, resulting in the looped blade with no tip, as illustrated in Fig.2b. This innovative design aims to mitigate the wasteful effects associated with wingtip vortices typically occurring at the tips of conventional blades. In this conceptual design, the geometry of the F29 propeller serves as the reference propeller for comparison purposes in order to assess the performance improvements introduced by the T-JBT propeller.

Table 1: Propeller specifications

	TUD-F29		T-JBT
J		0.4	
$V_\infty\ [m/s]$		20	
$D_p\ [m]$		0.308	
R_h/R_p		0.28	
AF	696.8		597.5
$Airfoil$		TUD-F29 Airfoil	
$\beta_{0.7R_p}\ [deg]$	20		30
$(c/R_p)_{Root}$	0.21		0.23
$(c/R_p)_{Tip}$	0.10		0.06

4.1 F29 Propeller

The F29 propeller geometry employed in this study as baseline is the TUD-F29 propeller which has four blades with a diameter $D_p = 304.8$ mm and blade pitch of $\beta_{0.7R_p} = 20$ deg. The propeller blade geometry characteristics, is illustrated in Fig.3a. The hub radius is $R_h = 0.28R_p$. This geometry was defined by the Fokker Aircraft Company for their internal F29 project [19]. The choice of this particular propeller for comparative analysis is based on the accessibility of both experimental data obtained by Tom Stokkermans [20] and numerical simulations data obtained by the previous work of the authors [21]. The propeller selected for comparison has been subjected to comprehensive testing an analysis, providing a dataset for a thorough examination of its aerodynamic characteristics and performance.

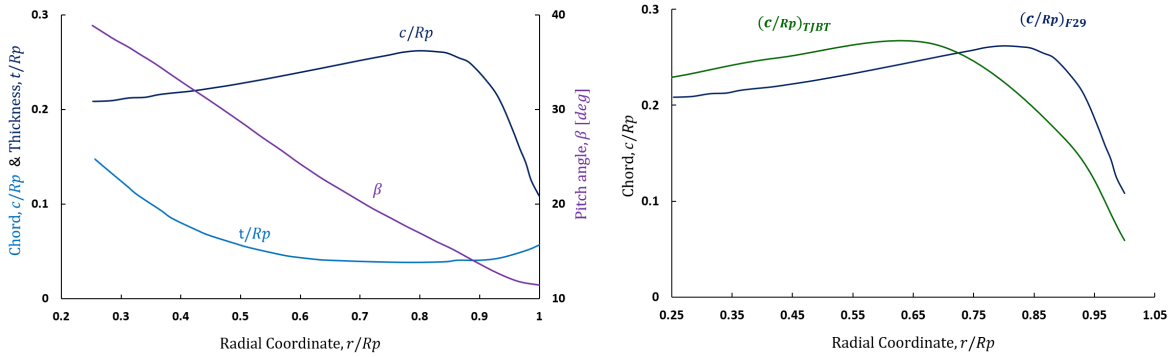

(a) F29 Blade characteristics

(b) Chord distribution comparison

Figure 3: Propellers characteristics : a) F29 Blade characteristics b) Chord distribution comparison

4.2 T-JBT Propeller

The T-JBT configuration consists of two looped blades featuring a constant pitch angle. Each looped blade is formed by joining two conventional blades at their mid-plane, resulting in a forward blade (FB) and rearward blade (RB) in relation to the rotation direction of the propeller, as depicted in the Fig.4a. The initial choice for the comparative study involves employing 2 looped blades, equivalent to 4 conventional blades.

The airfoils are arranged on predetermined stacking line (distribution line), incorporating specific parameters such as chord, thickness, and pitch (see Fig. 4c). The airfoil aerodynamic center ($a.c = 0.26c$) was determined using XFOIL and aligned on the stacking line. The airfoils are positioned such that they face the airflow directly with no angle except from the local angle of attack , as illustrated in Fig. 4d. Symmetrical airfoil was employed at the tip. The distribution lines of the FB and RB are connected at the plane half way from the two blades, as shown in Fig. 4. In this phase of the investigation, no attempts were made to optimize the blade geometry parameters or the number of blades. Both the pitch and chord distributions are intentionally set to be identical for both forward and rearward blades.

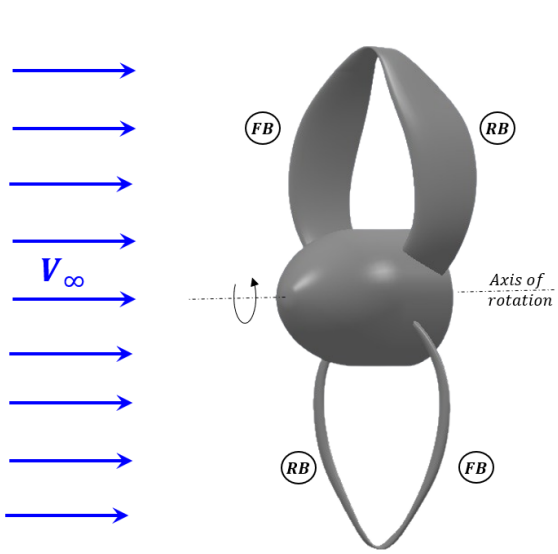

(a) Airflow and propeller rotation. Forward blade (FB) and rearward blade (RB) relative to the direction of rotation

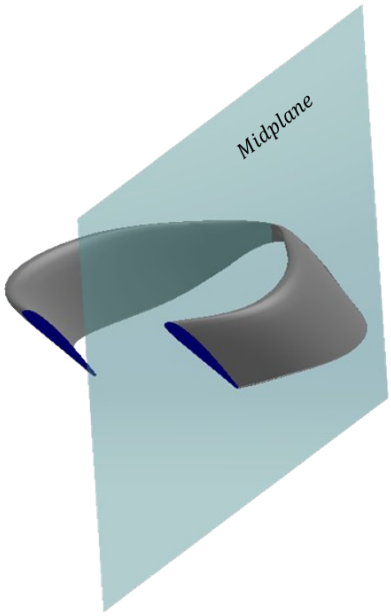

(b) Blade section at $r/R_p = 0.12$ and Midplane

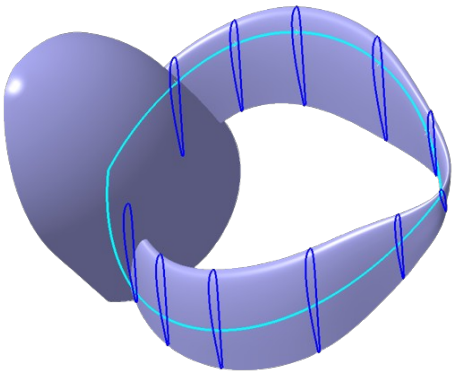

(c) Airfoil positioning along the blade

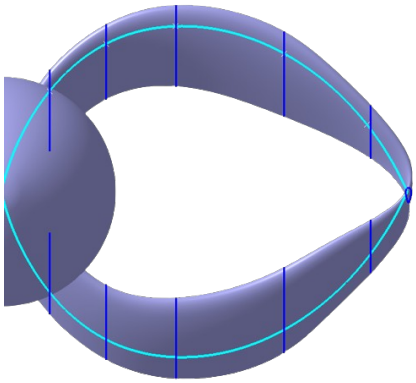

(d) Airfoils at different locations

Figure 4: T-JBT propeller with a) Airflow and propeller rotation. Forward blade (FB) and rearward blade (RB) relative to the direction of rotation, b) Blade section at $r/R_p = 0.12$ and Midplane, c) Airfoils positioning along the blade, d) Airfoils at different locations

5 Numerical Method

5.1 Physical Setup

The numerical simulation was conducted using URANS coupled with $k-\omega$ SST turbulence model [22, 23]. A mesh motion was employed to compute the unsteady flowfield generated by the propeller. This choice was driven by the high accuracy of the method in addressing the complexities of problems involving moving components [24]. In the Sliding Mesh approach, the cell zones rotate in discrete increments relative to each other along the mesh interface. Given the inherently unsteady nature of the flow in this problem, a transient condition is essential to capture the dynamic behavior accurately.

Time Step Calculation

To accurately capture the flow characteristics of the propeller, the time step was meticulously calculated, taking into account the operating conditions of the propeller. This careful consideration ensures that the time step is suitable for resolving the turbulent features of the flow, allowing for an accurate representation of the propeller

aerodynamic behavior. The the time step size (Δt) was calculated using the Equation 6, that was derived in the previous works by the authors [21].

$$\Delta t = \frac{2\pi}{\omega B \Delta d} \tag{6}$$

where ω is the rotational speed in rad/s, B is the number of blades and Δd is the single blade passing subdivisions.

Validation of the numerical setup for the isolated F29 propeller

The numerical setup was initially subjected to validation against experimental data obtained from research conducted by Stokkermans at the Technical University of Delft [19], utilizing the propeller (F29) and identical operating conditions (see Fig. 5). Further details regarding the validation process and discussion can be found in previous works by the authors (K. Combey et al. [21]). The average difference between the experimental and numerical predictions for the thrust coefficient is $\Delta C_T = 0.018$. Consequently, these comparisons instill a degree of confidence in the numerical setup accuracy.

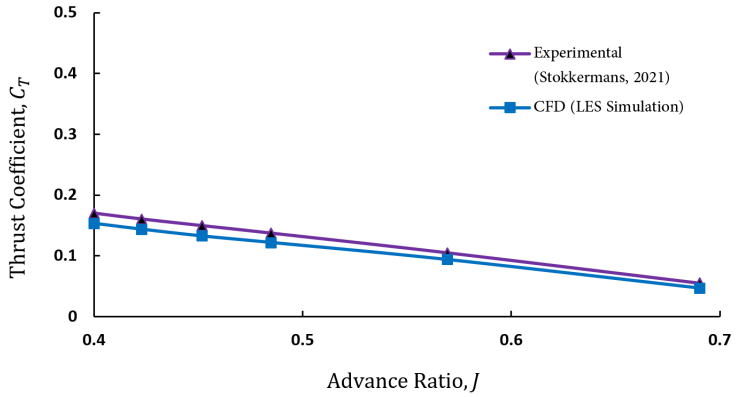

Figure 5: Comparison of the isolated propeller thrust coefficient, obtained from the numerical simulation with experimental data

5.2 Computational Domain

A rotating propeller problem requires two domains, which includes the rotating domain (RD) and the stationary or surrounding domain (SD). These domains serve different purposes in properly simulating the behavior of the propeller induced flow and its interaction with the surrounding airflow. The SD is extended 10 times the propeller radius $(10R_p)$ behind the propeller (see Fig. 6). This enables the visualization of the wake of the propeller and was sufficient to have far boundary and freestream conditions.

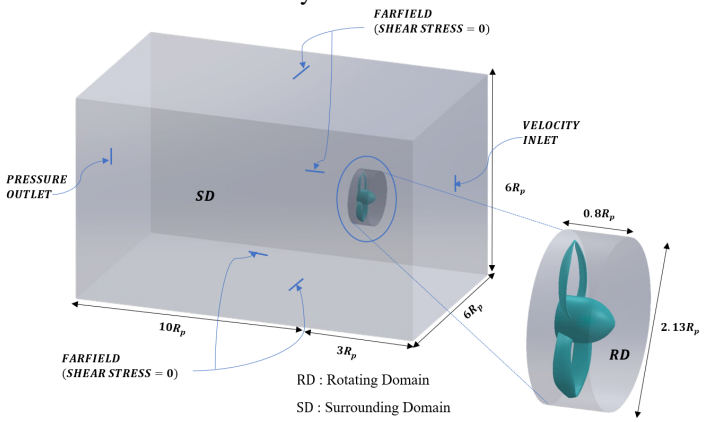

Figure 6: Computational domain and boundary conditions

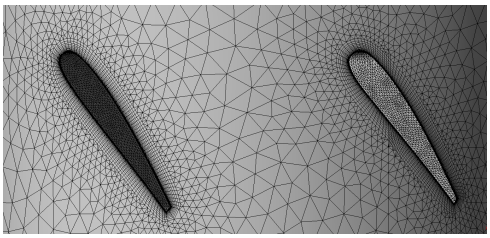

Figure 7: Unstructured mesh, showing the inflation layers around the blades at the section $r/R_p = 0.28$

5.3 Boundary Conditions

All simulations were performed under a freestream velocity of 20 m/s and an advance ratio (J) of 0.4. To allow the mesh motion of the RD, interfaces were created between the rotating and stationary domains, and treated as symmetry. These interfaces allowed fluid to flow from the inlet of SD, pass through the RD, and reach the outlet of SD. The inlet and outlet were set as a velocity inlet and pressure outlet, respectively, while all other sides of the SD were set as farfield boundaries imposing zero shear stress, as depicted in Fig. 6. The propeller surfaces were all set as no slip wall.

5.4 Grid generation and Grid Independence

In this study, an unstructured grid was constructed by means of ANSYS Meshing. The grid density was controlled by face sizing and body refinement. The blades were surrounded by 20 inflation layers with growth rate of 1.2 and first layer thickness, which serves the purpose of setting the y^+ value of 0.8.

Table 2: Number of elements and nodes of the coarse, medium, med-fine, fine and very-fine meshes

Meshes	Coarse	Medium	Med-fine	Fine	Very-Fine
Elements	755,494	1,159,0645	2,368,645	8,583,596	12,896,061
Nodes	245,933	396,947	853,799	2,368,645	5,056,237

Mesh independence study was conducted to ensure that the solution does not depend on the mesh size. This process allows for creating a mesh with sufficient quality to achieve reliable and accurate results while minimizing computational time and achieving good solution convergence. For this purpose, five different meshes, ranging from relatively coarse to very-fine, have been generated, as outlined in Table 2. The methodology for this process is detailed in prior works by the authors (K. Combey et al. [21]).

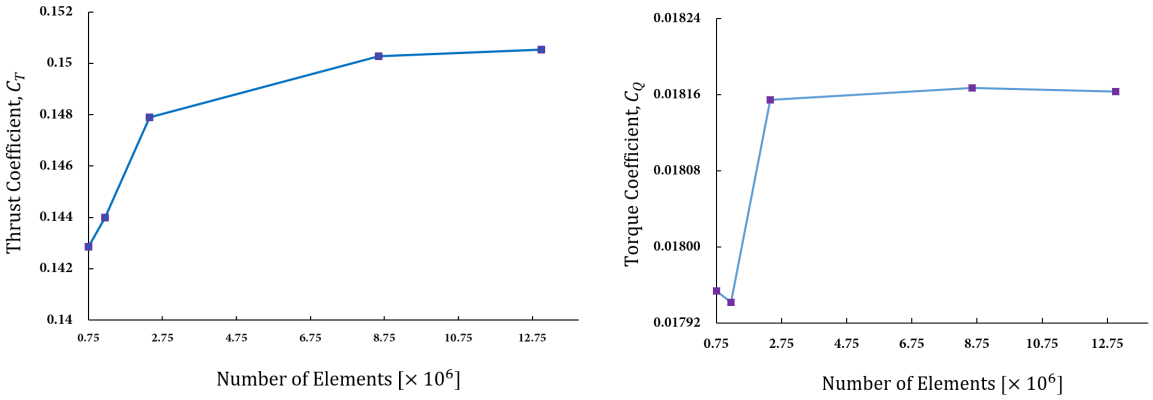

(a) Thrust Coefficient

(b) Mesh independence study for isolated propeller

Figure 8: Mesh independence study for isolated propeller

To evaluate the mesh independence, the thrust coefficient, C_T, and torque coefficient, C_Q were monitored. As shown in Fig 8, the variation of the monitored quantities become quasi-constant after certain number of elements. The thrust coefficient increases by 1.6% and torque coefficient by 0.07% when the number of elements was increased from 2.4 to 8.6 million, while the variation in both coefficients becomes relatively negligible, with only 0.1% and 0.02% variations, respectively when the number of elements increase from 8.6 to 12.9 million. These results suggest that the 8.6 million-element mesh is sufficient to yield accurate results with reduced computational costs. Detailed mesh setup information for the selected fine mesh element is presented in Table 3, and the grid structure showing the the inflation layers around the blades is illustrated in Fig. 7.

Table 3: Mesh setup of the optimal mesh

Mesh options	Parameters
Volume mesh	Tetrahedral
Element size and maximum size	4×10^{-2} m
Minimum face size	4×10^{-4} m
Inflation option	First Layer Thickness
First layer height	1.3×10^{-5} m
Maximum layers/Growth rate	20/1.2

6 Results and Discussion

6.1 Performance Analysis

The thrust (C_T) and torque (C_Q) coefficients were calculated for both the toroidal shape T-JBT and conventional F29 propellers and are presented in the Table 4. The two propellers were set at the same operating condition where the advance ratio $J = 0.4$ and the freestream velocity $V_\infty = 20m/s$. At this condition, the predicted C_T and C_Q coefficients increased by nearly twice the values of F29.

Table 4: Performance parameters

	C_T	C_Q
F29	0.149	0.018
T-JBT	0.212	0.039

The T-JBT propeller generated 42% more C_T compared to that of the F29 propeller. In addition, the T-JBT shows to be more efficient is producing torque. This significant improve in the performance is firstly associated with the absence of tip vortices for the looped-blade shape. In fact, the continuous blade design of the T-JBT propeller prevents wingtip vortices, which would normally cause induced drag on a traditional propeller blade. This reduction in drag losses enables more net torque to be generated. The induced velocity on the inner loop surface of the rearward blade caused by the forward blade, have a beneficial influence on the angle of attack on the inner surface, and therefore increasing thrust. The connected-tips of the T-JBT also changes flow characteristics compared to a finite one, potentially improving thrust and torque. In this initial design of the T-JBT propeller, the thickness ratio is constant from the R_h until the R_p, this avoid the thin blade lift penalties at the joint. Although a lower AF tends to reduce lift, the T-JBT unique design characteristics compensate through other aerodynamic mechanisms, resulting in higher lift overall.

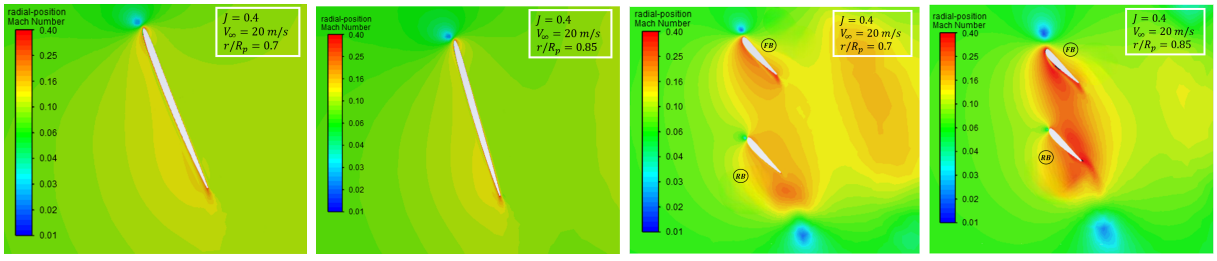

(a) (b) (c) (d)

Figure 9: Mach number distribution for a) F29 at $r/R_p = 0.7$ b) F29 at $r/R_p = 0.85$ c) T-JBT at $r/R_p = 0.7$ and d) T-JBT at $r/R_p = 0.85$

6.2 Flow Visualisation

Flow visualizations shown in Fig.9 to Fig.11 indicate significant differences in the flow fields over the two propellers. The flow field around the F29 blade, shown in Fig.9a and Fig.9b, appears to be attached to the suction side of the blade at the two radial positions. Meanwhile, in the flow field depicted in Fig.9c and Fig.9d of the

T-JBT propeller, flow interaction between FB and RB is observed. Generally, the flow is greatly accelerated on the suction sides of both FB and RB, leading to a drop in pressure values on the suction sides and resulting in higher differential pressure. Consequently, this results in high propeller performance. In Fig. 9d, relatively two small laminar separation bubbles appear on the suction side of the FB, followed by flow reattachment due to the generated turbulent boundary layer. The induced flow from the FB will modify the nature of the flow seen by the high-pressure side of the RB, thus resulting in a change in the angle of attack. In addition, Fig. 10 shows the gradual increase in speed from the root to the tip, which is due to the tangential speed.

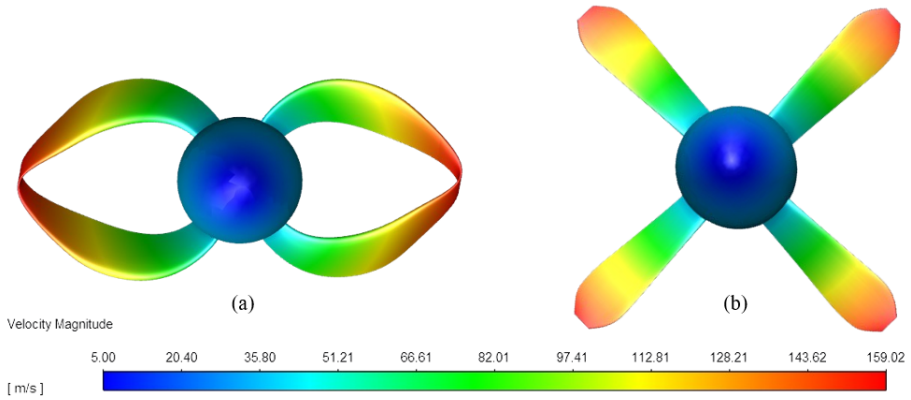

Figure 10: Gradual velocity distribution over the propellers for a) T-JBT and b) F29

In analyzing the velocity distribution downstream for both propellers, as illustrated in Fig. 11, it is evident that the wake velocities behind the toroidal-shaped propeller exceed those observed with the conventional propeller. Specifically, the T-JBT propeller generates a 42% higher thrust production compared to the F29 propeller. This enhanced thrust generation necessitates the acceleration of a greater air mass flow rate rearward, leading to increase wake velocities. The absence of wingtip vortices in the T-JBT design contributes to reduced swirl losses, enabling a more efficient conversion of rotor power into useful axial induced velocity rather than tangential speed. Moreover, due to the looped-blade design, the induced flow from the forward blade passes over the rearward blade, potentially enhancing its own induced flow. This phenomenon results in an increased axial velocity component behind the T-JBT propeller, leading to higher overall velocities in the wake. Additionally, the wake become confined between the looped blades, creating a nozzle effect and accelerating the flow further.

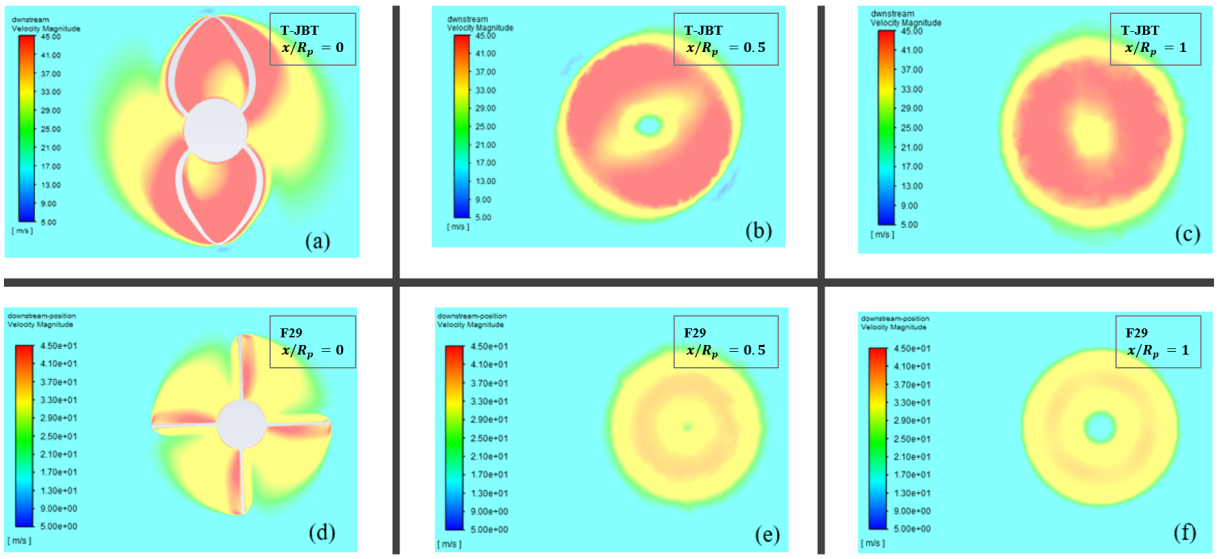

Figure 11: Velocity distribution at different position behind the propellers: a) $r/R_p = 0$, b) $r/R_p = 0.5$, c) $r/R_p = 1$ for the T-JBT propeller and d) $r/R_p = 0$, e) $r/R_p = 0.5$ e) $r/R_p = 1$ for the F29 propeller

7 Conclusion

This study investigated the aerodynamic performance of the Toroidal Joined Blade Tips (T-JBT) propeller, a proposed new design with looped blades formed by two conventional blades connected at their tips. Inspired by the potential to reduce propeller noise by eliminating tip vortices, numerical simulations were performed and compared with a classical propeller to analyze its aerodynamic performance. The obtained results under the considered operating conditions show that the T-JBT propeller has better performance than the conventional propeller, producing more thrust and torque. This feature is due to the looped blade design, where there is no tip; therefore, the losses decrease while the aerodynamic performance increases. Moreover, the presence of the blade creates a channel effect that accelerates the flow in the wake of the propeller. This accelerated air flow will, therefore, change the flow characteristics of anything located in the wake region, including propeller for multirotor eVTOLs. The findings fall within the context of urban air mobility, where innovative solutions are sought to address the challenges of increased energy demand and environmental impact. The T-JBT propeller can be applied in eVTOL aircraft and promises to revolutionize urban transportation.

Since this study primarily addresses the initial design of the T-JBT propeller, further research is necessary to optimize its geometry. Additionally, exploring the acoustic performance of this toroidal blade configurations will deepen our understanding and help guide the practical integration of UAM technologies, potentially revolutionizing urban transportation.

Conflicts of Interest

The authors declare that there are no known conflict of interest associated with this publication.

Nomenclature

eVTOL	:	Electric Vertical Take-Off and Landing	C_T	:	Thrust coefficient
DEP	:	Distributed Electric Propulsion	CQ	:	Torque coefficient
UAM	:	Urban Air Mobility	CP	:	Power coefficient
T-JBT	:	Toroidal Joined Blade Tips	V_∞	:	Freestream velocity
J	:	Advance ratio	n	:	Propeller speed
AF	:	Activity factor	Dp	:	Propeller diameter
FB	:	Forward blade	Rp	:	Propeller radius
RB	:	Rearward blade	ρ_∞	:	Freestream density
T	:	Thrust	Q	:	Torque

References

[1] Aleksandar Bauranov and Jasenka Rakas. Designing airspace for urban air mobility: A review of concepts and approaches. *Progress in Aerospace Sciences*, 125(100726), 2021. https://doi.org/10.1016/j.paerosci.2021.100726.

[2] Giuseppe Palaia, Karim Abu Salem, Vittorio Cipolla, Vincenzo Binante, and Davide Zanetti. A conceptual design methodology for e-vtol aircraft for urban air mobility. *Applied Sciences*, 11(10815), 2021. https://doi.org/10.3390/app112210815.

[3] Jeff Holden and Nikhil Goel. Fast-forwarding to a future of on-demand urban air transportation. Technical report, Tech. rep. Uber Elevate, 2016. https://evtol.news/__media/PDFs/UberElevateWhitePaperOct2016.pdf.

[4] Adam Cohen and Susan Shaheen. Urban air mobility: Opportunities and obstacles. *International Encyclopedia of Transportation*, pages Pages: 702–709, 2021. https://doi.org/10.1016/B978-0-08-102671-7.10764-X.

[5] Christopher Courtin; Ara Mahseredjian; Annick J. Dewald; Mark Drela and John Hansman. A performance comparison of estol and evtol aircraft. Online Event, August 2021. American Institute of Aeronautics and Astronautics, ARC. https://doi.org/10.2514/6.2021-3220.

[6] Omer A Elsayed, Waqar Asrar, Ashraf A Omar, and Kijung Kwon. Evolution of naca23012 wake vortices structure using piv. *Journal of Aerospace Engineering*, 25(1):10–20, 2012. https://doi.org/10.1061/(ASCE)AS.1943-5525.00001.

[7] Khaoula Qaissi, Omer Elsayed, Mustapha Faqir, and Elhachmi Essadiqi. Performance enhancement analysis of a horizontal axis wind turbine by vortex trapping cavity. *Journal of Energy Resources Technology*, 144(3):031303, 2022. https://doi.org/10.1115/1.4052980.

[8] Khaoula Qaissi, Omer Elsayed, Mustapha Faqir, and Elhachmi Essadiqi. Optimization of the aeroacoustics and aerodynamics of a wind turbine airfoil with serrations using multi-criteria decision making. In *2023 10th International Conference on Recent Advances in Air and Space Technologies (RAST)*, pages 1–5. IEEE, 2023. https://doi.org/10.1109/RAST57548.2023.10197890.

[9] Hyun D. Kim; Aaron T. Perry and Phillip J. Ansell. A review of distributed electric propulsion concepts for air vehicle technology. Cincinnati, Ohio, July 2018. AIAA/IEE Electric Aircraft Technologies Symposium, IEEE. https://ntrs.nasa.gov/citations/20180004730.

[10] Hyun D. Kim ; Aaron T. Perry and Phillip J Ansell. Progress in distributed electric propulsion vehicles and technologies. Technical report, NTRS - NASA Technical Reports Server, 2020. https://ntrs.nasa.gov/citations/20200011461.

[11] AGARD and Von Kärmän Institute. *The Aerodynamics of V/STOL Aircraft*. Technical Editing and Reproduction Ltd, Rhode-Saint-Genese, Belgium,, 1968. Lecture Series https://apps.dtic.mil/sti/tr/pdf/AD0688921.pdf.

[12] Johnny T Doo, Marilena D Pavel, Arnaud Didey, Craig Hange, Nathan P Diller, Michael A Tsairides, Michael Smith, Edward Bennet, Michael Bromfield, and Jessie Mooberry. Nasa electric vertical takeoff and landing (evtol) aircraft technology for public services - a white paper. 2021. https://ntrs.nasa.gov/api/citations/20205000636/downloads/2021-08-20-eVTOL-White-Paper-Final_V48.pdf.

[13] Steelpillow. Aircraft wing configurations, 2023. Wikimedia Commons, Under Creative Commons Attribution-ShareAlike License & CC0 License; https://commons.wikimedia.org/wiki/User:Steelpillow/Aircraft (Last Modified : April 5, 2023) [Accessed: January 14, 2024].

[14] Steelpillow. Closed wing, 2023. Wikipedia, Under Creative Commons Attribution-ShareAlike License 4.0; https://en.wikipedia.org/wiki/Closed_wing (Last Modified : November 28, 2023)[Accessed: January 14, 2024].

[15] Jianwei Sun, Koichi Yonezawa, Eiji Shima, and Hao Liu. Integrated evaluation of the aeroacoustics and psychoacoustics of a single propeller. *International Journal of Environmental Research and Public Health*, 20(3), 2023. https://doi.org/10.3390/ijerph20031955.

[16] Alexandre Capitao Patrao, Daniel Lindblad, and Tomas Grönstedt. Aerodynamic and aeroacoustic comparison of optimized high-speed propeller blades. In *2018 Joint Propulsion Conference*, 2018. https://doi.org/10.2514/6.2018-4658.

[17] MIT Lincoln Laboratory. Toroidal propeller. Technical report, Massachusetts Institute of Technology, 2022. https://www.ll.mit.edu/sites/default/files/other/doc/2023-02/TVO_Technology_Highlight_41_Toroidal_Propeller.pdf.

[18] Ralph D Kimberlin. *Flight testing of fixed wing aircraft*, chapter 6, pages 67–68. AIAA, 2003. https://doi.org/10.2514/5.9781600861840.0063.0068.

[19] Tom Caton Arnaud Stokkermans. *Aerodynamics of Propellers in Interaction Dominated Flowfields : An Application to Novel Aerospace Vehicles*. PhD thesis, Delft University of Technology, 2020. https://pure.tudelft.nl/ws/portalfiles/portal/84548703/Stokkermans_TCA_PhDthesis.pdf.

[20] Tom C. A. Stokkermans, Daniele Usai, Tomas Sinnige, and Leo L. M. Veldhuis. Aerodynamic interaction effects between propellers in typical evtol vehicle configurations. *Journal of Aircraft*, 58, 2021. https://doi.org/10.2514/1.C035814.

[21] Kangni Combey, Omer A. Elsayed, Khaoula Qaissi, and Mustapha Faqir. Numerical analysis of multirotor aerodynamic interactions in one-after-another configuration. In *Delft International Conference on Urban Air Mobility, DICUAM-2024*, Delft, Netherlands, March 2024. TUD. (Under Review).

[22] Florian R Menter. Two-equation eddy-viscosity turbulence models for engineering applications. *AIAA journal*, 32(8):1598–1605, 1994.

[23] Florian R Menter, Martin Kuntz, Robin Langtry, et al. Ten years of industrial experience with the sst turbulence model. *Turbulence, heat and mass transfer*, 4(1):625–632, 2003.

[24] ANSYS. *ANSYS Fluent Theory Guide*. Release 12.0 © ANSYS, Inc, 2009. https://www.afs.enea.it/project/neptunius/docs/fluent/html/th/node1.htm.